Photodiagnosis and
Photodynamic
Therapy

Official Journal
of the European Platform
for Photodynamic Medicine

Vol 7 No 3 September 2010 ISSN 1572-1000

IN THIS ISSUE:
• PDT in cancer of oesophagus vs PDT with chemotherapy,
  and chemotherapy alone
• PDT for cervical intraepithelial neoplasia
• Reduction of cutaneous photosensitivity by application of
  ointment containing ferrous or cobalt ions
• Targeted laryngeal PDT

In vivo temporal evolution of ALA-induced normalized fluorescence at different anatomical locations of oral cavity: Application to improve cancer diagnostic contrast and potential

Rupananda Jayachandra Mallia PhD[a,*], Narayanan Subhash PhD[a], Paul Sebastian MS[b], Rejnish Kumar MD[c], Shiny Sara Thomas MSc[a], Anitha Mathews MD[d], Jayaprakash Madhavan MD[e]

[a] Biophotonics Laboratory, Centre for Earth Science Studies, Akkulam, Thuruvikkal PO, Trivandrum 695031, Kerala, India
[b] Division of Surgical Oncology, Regional Cancer Centre, Trivandrum 695011, India
[c] Department of Radiation Oncology, Regional Cancer Centre, Trivandrum 695011, India
[d] Department of Cytopathology, Regional Cancer Centre, Trivandrum 695011, India
[e] Department of Radiotherapy, Regional Cancer Centre, Trivandrum 695011, India
Available online 24 July 2010

Summary
Background: The focal goal of this study is to identify optimal accumulation periods for ALA-induced PpIX in different healthy anatomical sites of human oral cavity and different types of abnormal mucosa to improve the accuracy of the clinical applications such as photodiagnosis and tissue grading.
Materials and methods: Laser-induced fluorescence (LIF) emission spectra, with excitation at 404 nm from a diode laser, were recorded with a miniature fiber-optics spectrometer from 13 anatomical sites of oral mucosa in 15 healthy volunteers and 30 suspicious sites in 15 patients after topical application of 0.4% 5-ALA solution for 15 min. The optimal accumulation time in different anatomical sites of healthy subjects and abnormal tissues were determined by studying the temporal variation in normalized fluorescence intensities (NFI) at 635, 685 and 705 nm.
Results and discussions: In masticatory anatomical locations such as (gingival and hard palate) and in lining mucosa (inner lip, soft palate, floor of mouth, transition to floor of mouth, alveolus and ventral tongue) except vermillion border of lip (VBL) of healthy subjects (designated as group I), it was observed that optimum time for maximum accumulation of PpIX is 90 min. In comparison, for lateral side of tongue (LST) and dorsal side of tongue (DST) tissues (designated as group II), maximum accumulation of PpIX was observed in 150 min of ALA application. For diverse grade lesions of group I mucosa in patients, maximum accumulation of PpIX was observed in 90 min, whereas, in group II mucosa the optimum accumulation time was 150 min as in the case of healthy mucosa. Further, between different grades oral mucosa, maximum variation in NFI take place at these optimal time periods.

* Corresponding author. Tel.: +91 471 2511640; fax: +91 471 2442280.
  E-mail address: jrmallia@cessind.org (R.J. Mallia).

Conclusions: The determination of the optimum accumulation time of ALA in oral mucosa based on NFI helps to improve the diagnostic contrast and accuracy of oral cancer diagnosis, and to plan appropriate timing for ensuing PDT.

Introduction

Cancers affecting different anatomical sites of oral cavity now accounts for an estimated 274,000 new cases and 145,000 cases of fatality globally, each year [1]. Among the different optical spectroscopic techniques that are being tested presently for early detection of cancers and are on the verge of its application in a clinical environment along with other diagnostic adjunctive techniques, photodynamic detection (PDD) using photosensitizer is garnering a lot of attention via-a-vis laser-induced autofluorescence (LIAF) and diffuse reflectance spectroscopy (DRS) due to the clinical rationale that it can be followed up with therapeutic applications like photodynamic therapy (PDT).

PDD and PDT are reported to be sensitive and promising cancer diagnostic and therapeutic regimens where a photosensitizing drug accumulates and fluoresces preferentially in abnormal tissues and subsequently gets activated by visible light of an appropriate wavelength for selective destruction of abnormal tissues [2,3]. With the availability of photosensitizers that are more selectively retained in abnormal tissues, the reliability of optical diagnosis and therapy could be significantly enhanced. Moreover, it is advantageous if the photosensitizer is an endogenous molecule in terms of safety aspects and minimal side effects. In this perception, 5-ALA or ALA is an ideal choice, which is an endogenous molecule involved in the biosynthetic pathway of heme, gets intracellularly converted into the fluorescing compound PpIX [4,5]. ALA-induced PpIX is now a promising endogenous photosensitizer that could be used in non-invasive and non-toxic photodetection of cancer as compared to any other exogenous photosensitizers belonging to porphyrin, chlorin, texaphyrins and phthalocynine families [3,6,7].

ALA has been studied extensively as a photosensitizer for PDD and in PDT both in animal models [8–10] and in humans [11–13]. At present, ALA based PDD is a successfully established diagnostic method for of a variety of cancers, particularly oral cancers. Influence of different administration methods on PpIX fluorescence has been studied in detail by Ogasawara et al. to investigate optimal administrating method for ALA [14]. Vaidyanathan et al. has investigated the *in vivo* kinetics of ALA-induced fluorescence in canine oral cavity at different doses and found that a dose of 25 mg/kg of ALA is sufficient for diagnostic purposes with minimal side effects during oral administration [15–17].

ALA penetrates into the superficial mucosal cells when applied topically [9,18,19] and generally considered as a good route for administration as it avoids systemic side effects, and induces only local photosensitization. Another key advantage of topical application is that it is time saving as compared to intravenous and oral administration [9]. Fluorescence imaging studies of PpIX induced after topical administration of ALA in the oral cavity of patients with squamous cell carcinoma (SCC) by Betz et al. has shown

that cancerous tissues have significantly higher PpIX fluorescence [20]. Leunig et al., performed semi-quantitative florescence study following topical application of ALA and observed a contrast of 10:1 between normal and neoplastic oral tissues within 60–120 min, allowing demarcation of tumor tissues even with naked eyes [21]. In an another clinical work, after topical application of 0.4% ALA and an incubation time of 60–150 min, fluorescence images in the red and green spectral range were acquired to discriminate neoplastic tissues from the surrounding normal tissues [22]. The kinetics of ALA-induced PpIX production in different tissues has also been studied by Stolic et al., using fluorescence spectroscopy [23].

Zheng et al. had designed an ALA mediated digitized fluorescence endoscopic imaging system for on-line image acquisition and developed an algorithm for fluorescence quantification that facilitates early detection of neoplasm in the oral cavity [24]. The preliminary clinical results showed that red to blue image intensity ratio of malignant mucosa is higher than benign mucosa, after topical application of 0.4% ALA solution. In another study they showed that red to green ratios are also useful for discrimination of malignant tissues from benign with good diagnostic accuracies [25].

With the establishment of ALA as a precursor of PpIX that is selectively retained within neoplastic/abnormal tissues, the reliability of optical diagnosis and therapy has been significantly enhanced. Since normal mucosa also uptakes the ALA initially, Van der Veen and co-workers using an animal model had suggested that the knowledge of optimal time at which maximum accumulation of PpIX takes place both in normal and abnormal tissues via heme cycle, is bound to further enhance the detection accuracy [9]. However, *in vivo* temporal evolution of PpIX fluorescence in different anatomical sites of human oral mucosa after topical application is not well attempted, understood and elucidated yet, which is very important as per the clinical stand-view. Based on the above said firm clinical rationale, we have attempted this particular study to find the optimal accumulation time of ALA-induced PpIX at different anatomical sites in healthy mucosa and in different grades of abnormal oral mucosa. Our assumption is that since the oral cavity contains different types of mucosa, which differ in histology and keratin content, there could be differences in ALA penetration time, accumulation rate, PpIX conversion efficiency and fluorescence emission. We define ''Optimum time'' as that accumulation time at which the maximum accumulation of ALA or ALA-induced PpIX takes place within a normal and abnormal mucosa as compared to another incubation/accumulation time, which in turn gives maximum contrast to differentiate these tissue grades, thereby increasing the diagnostic potential. This paper presents the results of *in vivo* fluorescence kinetics from 13 different anatomical locations of the oral cavity in healthy population after topical administration of ALA. The study also covers

measurements in different abnormal tissues viz. hyperplasia, dysplasia, and SCC of oral cavity for evaluating the optimum accumulation time of ALA-induced PpIX and its application in tissue differentiation as a proof of principle for the aforementioned hypothesis, and lays some useful groundwork for the prospective studies.

Materials and methods

Instrumentation

The laser-induced fluorescence and reflectance spectroscopy (LIFRS) system comprises of a diode laser (Stocker Yale Inc., Canada, 404 nm, 50 mw, CW) and a tungsten halogen lamp (Ocean Optics, Model: LS-1, USA) that could be switched alternately for recording of LIF and DR spectra of same tissue site, sequentially. A bifurcated optical fiber guides the light output to the oral tissue through a 3-m long fiber-optic probe that has a central fiber to deliver the excitation beam and six surrounding fibers (400 μm dia.) to collect LIF/DR emission. The probe tip is terminated in a stainless steel ferrule, 15 cm long and 6 mm dia., to enable sterilization before and after use. A black PVC sleeve of length 30 mm inserted at the probe tip maintains a fixed separation of 3 mm between the probe tip and the tissue sample and enhances the LIF/DR signal yield by providing optimum overlap between the excitation and collection areas. This opaque black sleeve also provides extra hygiene, as it is disposable after measurements in each patients/volunteers. The light emanating from the sample is delivered to a miniature fiber-optic spectrometer (Ocean Optics USB 2000FL VIS-NIR), connected to the USB port of a laptop computer. During fluorescence studies a long-wavelength pass filter (Schott GG420) was used to block the back-scattered laser light from entering the spectrometer. More technical details and schematic of the LIFRS system are described elsewhere [26,27].

Data acquisition and data processing

A fiber-optic light-coupler (Spectra Physics, USA, Hydrax) fixed on the laser head was used to focus the laser beam on to the fiber tip such that the output light projects a beam of Gaussian intensity profile on the tissue surface. In order to provide optimal signal output quality, the laser output power at probe tip was maintained at 1 mW during measurements by frequent monitoring with a power/energy meter (Ophir Optronics, Israel, Model: PE 10-V2). Slight pressure was applied on the lesion/mucosa with the sleeve tip of the probe to avoid ambient light from entering the detection system. After each set of measurements on patients/healthy volunteers, the sleeve was discarded and probe sterilized with boiling water. Subsequently, the entire probe was stored inside a plastic box containing formalin tablets for supplementary sterilization. The miniature fiber-optic spectrometer was fitted with a 600 lines/mm, 500 nm blazed grating for operation in the 360—1000 nm wavelength range. The detector used was a 2048-element, linear silicon CCD array and in conjunction with a 200-μm slit, the monochromator produced an optical resolution of 8 nm. The LIF spectra were acquired with the help of the OOI Base32 software (Ocean Optics, USA) that was configured to record the spectra, averaged for 40 scans, with a boxcar width of 10 nm and an integration time of 100 ms.

Prior to LIF and DR measurements, the background spectrum was recorded and the OOI Base32 software was configured to automatically subtract the same during each measurement. Considering the heterogeneous nature of oral cavity lesions, 15 sets of fluorescence measurements were taken from each suspicious lesion of the patient. Ten sets of LIF spectral measurements were taken from each mucosa/lesion in the 420—720 nm spectral window and the mean value was used in data analysis. Artifacts due to oxygenated hemoglobin absorption were noticed in the LIF spectra at 545 and 575 nm [26,27]. Various refining models have been used by different groups to correct these absorption dips and recover intrinsic autofluorescence spectra from the recorded fluorescence spectra [28,29]. However, we have used a first order approximation that involves division of LIF with the DR spectra from the same tissue site to remove the absorption artifacts [30,26].

The ability of using fluorescence intensity of peaks in discriminating different diseased tissue types from normal was tested by receiver operating characteristic (ROC) curve analysis [31,32]. In a ROC the sensitivity is plotted against (1-specificity) for different cut-off points. ROC allows the user to take a good decision of the effectiveness of different diagnostic methods without constraining him to single values of sensitivity and specificity, which largely depends on the chosen threshold [33]. Each point on the ROC plot represents a sensitivity/specificity pair corresponding to a particular decision threshold and one can easily predict the best methodology by simply noting the area under the curve (AUC). A test with perfect discrimination (no overlap) has a ROC plot that passes through the upper left corner of the plot (100% sensitivity, 100% specificity). The more accurately a methodology or technique separates the data types, the corresponding area under ROC curve (ROC-AUC) approximates to 1.

Study protocol and clinical measurements

The entire clinical study included 36 healthy volunteers, with no clinically observable lesions or inflammatory conditions in their oral cavity, and 48 patients, with measurements taken from 94 suspicious sites, having clinically low/high-risk lesions in their oral cavity. The major constraint in this study was on the availability of patients for ALA-induced temporal studies. Majority of the registered patients belonged to the age group of 60—70 years, with supplementary diseases like diabetics and blood pressure. Many of these claustrophobic patients did not want to stay without eating during prolonged period of usual tests and temporal spectral measurements after ALA administration, which could last for about next 4 h. Due to this reason out of aforementioned study population, 30 sites of 15 patients and 13 anatomical sites of 15 healthy volunteers only were available for ALA-induced PpIX kinetic studies. The 13 anatomical locations involve the mucosa from the right and left buccal mucosa, the gingiva, the upper and lower alveolus, the floor of mouth, the hard and soft plate, the dorsal tongue, the lateral border tongue, the ventral tongue, the inner lip, the

vermillion border of lip and the transition of tongue, and pictorial representation of different anatomical sites within human oral cavity is given elsewhere [26].

In each patient, an experienced head and neck clinician selects the suspicious lesions for spectral studies and records its visual imprint. Most of the patients studied had prolonged smoking or *pan* chewing habits whereas healthy volunteers were free of such habits and maintained good oral health or hygiene. As compared to our earlier study, histopathological analysis of biopsy samples showed that mucosa adjoining malignant sites in patients are not usually normal, but displayed varying degrees of epithelial dysplasia and hyperplasia. Therefore, instead of using LIAF data from apparently normal lesions of patients as control, we have used spectral data from the oral mucosa of healthy volunteers as control [26,27]. Spectral measurements were carried out at the outpatient clinic of the RCC, Trivandrum, India. Prior approval for the clinical trial and its protocol was obtained from the Ethics Committee of RCC. After explaining the modalities of the study, written informed consent was obtained from each patient/volunteer prior to enrolment.

Before commencement of autofluorescence measurements, the patients/volunteers were directed to hold 0.9% saline solution in their mouth for 2—3 min to reduce the effects of recently consumed food. The photosensitization of the oral mucosa was carried out by directing the patients and/or healthy volunteers to hold/rinse their oral cavity with 0.4% freshly prepared solution of ALA (Medac, Hamburg, Germany) (prepared by mixing 40 mg of ALA in 10 ml of distilled water) for 15 min [34,35], maintaining a continuous contact to the tissue or lesion of interest to ensure expected mucosal saturation [35,36]. ALA was selected for the study, as it is endogenous in nature and gets excreted from the body in less than 24 h of application, thereby eliminating whatever little side effects like skin photosensitivity that are reported [37,12]. A concentration 0.4% of ALA was selected as many researchers have shown that this concentration is ideal for diagnostic needs [24,25,35]. Measurements on patients and healthy volunteers were carried out in a dark room to avoid direct exposure to external light. The excitation power of the diode laser (405 nm) was kept very low around 1 mW at the fiber tip (which produces a irradiation of $0.02\,mW/cm^2$), to avoid skin photosensitization or side effects. The power at the fiber tip had been monitored and maintained at this low power level during the each set of measurements using the optical power meter to ensure this fact. The *in vivo* temporal measurements were performed at time intervals of 60, 90, 120, 150 and 210 min (or 90, 120, 150 and 210 min) ensuing ALA application depending on the tissue group. The optimum accumulation time was determined for different healthy anatomical sites and abnormal tissues by tracking the temporal variation in fluorescence intensity of PpIX and its precursors in Heme cycle at 635, 685 and 705 nm wavelengths.

In patients, incision biopsies were taken from the measurement sites after completion of *in vivo* temporal fluorescence measurements. The biopsy samples were fixed in 10% normal formalin and sent for histopathological analysis. Histology slides were prepared from the biopsies and classified by an experienced pathologist blinded to the fluorescence spectral results. In the case of healthy volunteers, visual inspection was carried out instead of biopsy. After
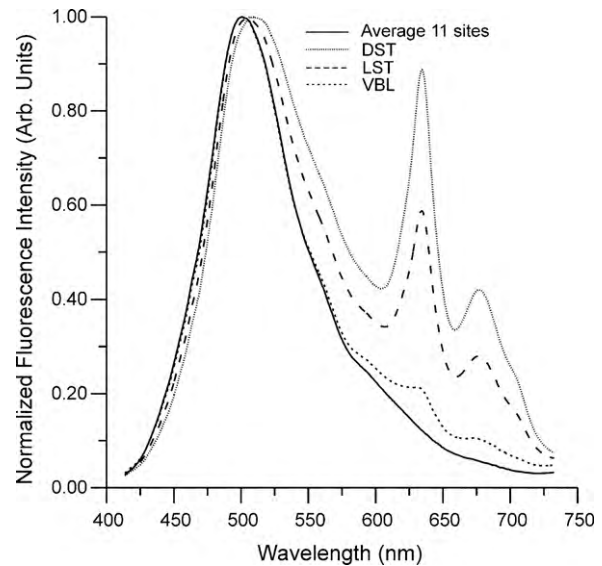

Figure 1 Mean LIAF spectra from the dorsal side of tongue (DST), lateral side of tongue (LST), and vermillion border of the lip (VBL) normalized to the autofluorescence intensity at 500 nm and compared with the mean spectrum from all 11 other sites of the oral cavity. DST, LST, and VBL spectra represent the mean of 15 measurements each in 36 volunteers, whereas the average normal spectra relates to the mean of 15 measurements each at 11 sites in these volunteers.

classification, spectroscopic data were correlated with the histopathological findings. Independent Student's *t*-test was performed on the observed fluorescence intensities to assess their statistical significance in discerning different types of mucosa.

Results

LIAF spectral features of anatomically different healthy oral mucosa

The broad autofluorescence peak seen in the LIF spectra at 500 nm is characteristic of all epithelial tissues. Fig. 1 represents the mean *in vivo* LIF spectra recorded from 13 anatomical sites of oral cavity measured from a population of 36 healthy volunteers normalized to the 500 nm peak intensity. The dorsal side of tongue (DST), lateral side of tongue (LST) and vermillion border of lip (VBL) tissues show emissions at 635, 685 and 705 nm that appear to be as due to the presence of porphyrins, with the DST tissues showing prominent peaks as compared to LST and VBL. Whereas, in all other healthy anatomical tissues these porphyrin-like emissions are absent and show almost a similar spectral profile. Therefore, an average of these is used to represent the healthy spectra for all these anatomical sites.

Optimum accumulation time for ALA-induced PpIX in healthy oral mucosa

The uptake of ALA and ensuing accumulation of PpIX at different anatomical sites of the oral cavity was studied by monitoring the LIF spectral changes over 210 min duration
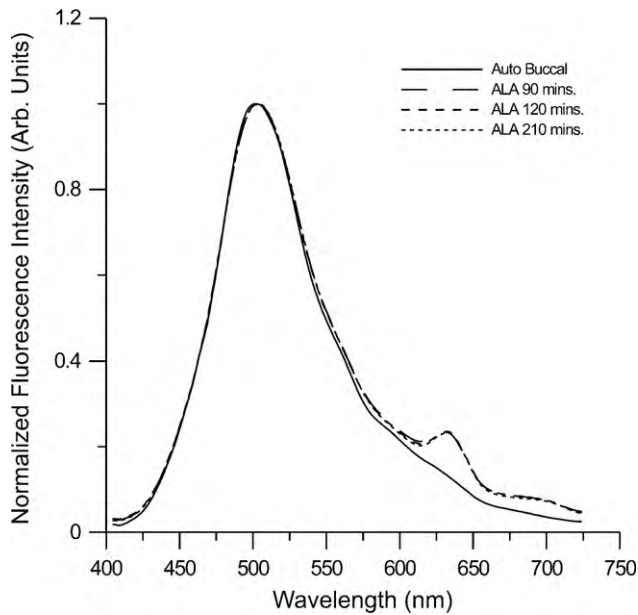
Figure 2 The mean normalized LIF spectra from the buccal mucosa of the healthy volunteers before and after topical application of 0.4% 5-ALA solution for 15 min.
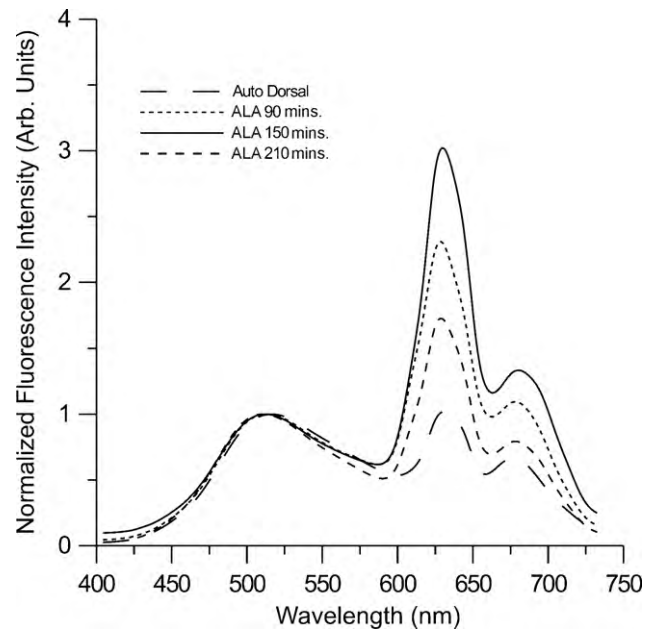

Figure 3 Temporal variation in the normalized LIF spectra from the DST in healthy volunteers before and after topical application of 0.4% 5-ALA solution for 15 min.

following topical application of ALA. A dismal fall in intensity at 500 nm is observed, while the PpIX emission intensities at 635 and 705 nm get enhanced. An additional peak was noticed in the LIF spectra at 685 nm, which makes the 705 nm emission peak appear broadened. Figs. 2 and 3 show the mean LIF spectra normalized to the intensity of the autofluorescence peak (500 nm) at different time intervals from the buccal mucosa and DST, respectively, in healthy volunteers. Spectral intensity changes due to PpIX accumulation is obvious usually after 60 min of topical ALA application. The optimum time for maximum accumulation at different sites was determined by tracking the normalized fluores-

cence intensity (NFI) variations in Figs. 1 and 2. Table 1 lists the time at which maximum accumulation of ALA-induced PpIX occurs in different anatomical sites of oral cavity.

In anatomical locations such as masticatory mucosa (the gingival and hard palate) and lining mucosa (the inner lip, softpalate, floor of mouth, transition to floor mouth, alveolus and ventral tongue), it is observed that maximum enhancement in intensity occurs at 635, 705 and 685 nm in 90 min of ALA application. Fig. 4a—d shows the temporal variation in the mean normalized intensities at 635, 685 and 705 nm for buccal, DST, LST and soft palate, respectively,

Table 1 Maximum accumulation time of ALA-induced PpIX in different anatomical sites of oral cavity observed by monitoring temporal variation of the normalized fluroscence intensities at 635, 685 and 705 nm after topical application of 0.4% 5-ALA solution.

| Tissue groups	Oral anatomical sites	Optimal PpIX accumulation (min)	Intensity at 635 nm	Intensity at 685 nm	Intensity at 705 nm
Group I	Alveolus	90	0.27 ± 0.15	0.08 ± 0.02	0.07 ± 0.02
	Buccal mucosa	90	0.23 ± 0.12	0.08 ± 0.03	0.07 ± 0.01
	Gingiva	90	0.31 ± 0.06	0.12 ± 0.04	0.11 ± 0.04
	Ventral tongue	90	0.39 ± 0.06	0.11 ± 0.02	0.10 ± 0.03
	Hardpalate	90	0.29 ± 0.10	0.12 ± 0.03	0.11 ± 0.04
	Softpalate	90	0.27 ± 0.09	0.14 ± 0.06	0.12 ± 0.05
	Floor of mouth	90	0.26 ± 0.13	0.08 ± 0.06	0.07 ± 0.01
	TFM	90	0.27 ± 0.08	0.08 ± 0.05	0.07 ± 0.03
	Inner lip	90	0.37 ± 0.05	0.21 ± 0.03	0.11 ± 0.03
	Group I average	90	0.30 ± 0.05	0.11 ± 0.02	0.09 ± 0.03
Group II	VBL	150	0.38 ± 0.04	0.10 ± 0.03	0.09 ± 0.05
	DST	150	2.98 ± 0.34	1.20 ± 0.23	0.84 ± 0.21
	LST	150	1.56 ± 0.22	0.49 ± 0.10	0.43 ± 0.09
	Group II average	150	1.64 ± 1.30	0.60 ± 0.55	0.42 ± 0.37
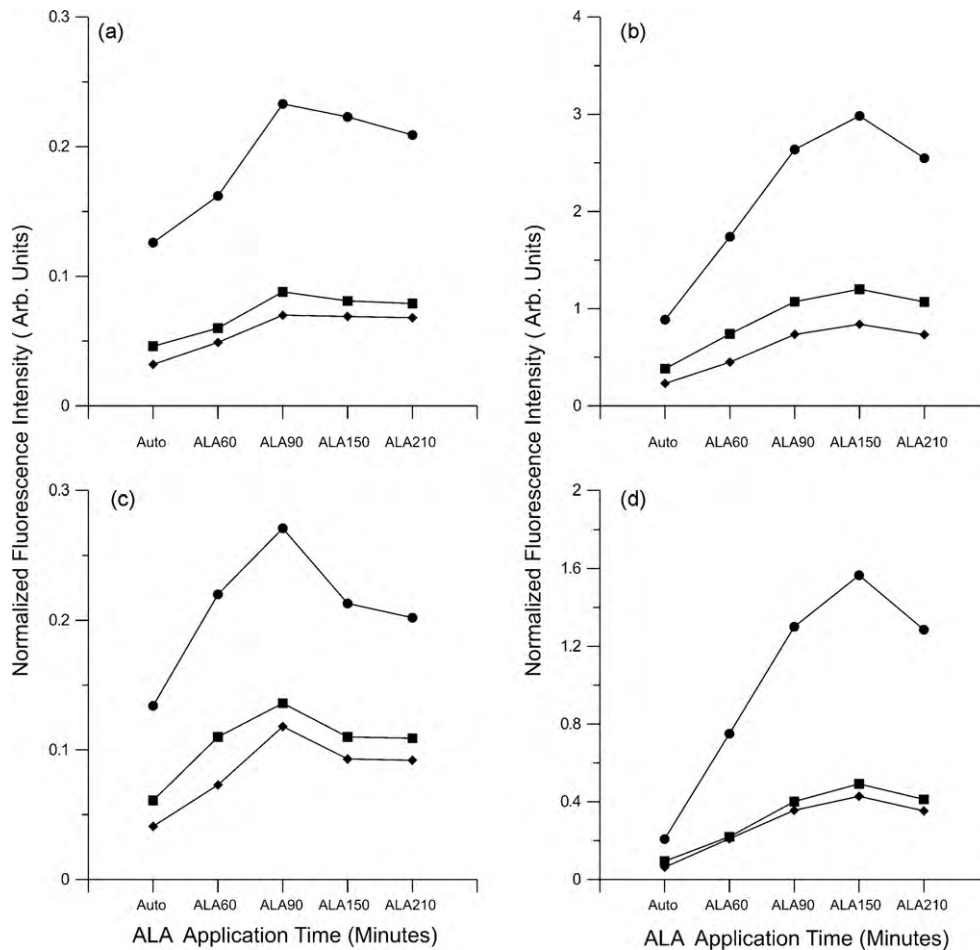
Figure 4 Temporal variation in the mean normalized fluorescence intensities (NFI) at 635, 685 and 705 nm of (a) buccal, (b) DST, (c) LST, and (d) soft palate mucosa for different periods of accumulation after topical application 0.4% 5-ALA.

after ALA application. The optimum time of accumulation of PpIX in these tissues can be understood from the shape of the graph. It is noticed that the peak intensity for these mucosa are in same range (Table 1). However, in the case of VBL, LST and DST mucosa, maximum enhancement was seen only after 150 min of ALA application. The DST and LST sites have larger variations in the normalized peak intensities as compared to all other anatomical sites; they are also unique due to higher accumulation time of PpIX. However, for VBL the accumulation time is same as that of DST and LST, but the intensity variation is similar to those of other sites. Therefore, it appears that for all anatomical locations, excluding DST, LST and VBL, the normalized intensities are interchangeable for diagnostic purposes using ALA-induced porphyrin fluorescence. After the optimal accumulation time is reached, normalized intensities gradually decrease depending on the tissue type. In buccal mucosa and other anatomical sites this decrease is very small with time, whereas it is faster at DST and LST sites.

LIAF spectral features of abnormal mucosa

In abnormal tissues (SCC and dysplasia) from anatomical sites other than DST, LST and VBL, besides autofluorescence peak at 500 nm, two peaks around 635 and 705 nm due to

PpIX emission are observed. Fig. 5 shows the mean *in vivo* LIAF spectra of different tissue types, normalized to the intensity of the autofluorescence peak. In lesions pathologically diagnosed as SCC, the peak at 635 nm is very prominent as compared to dysplastic tissues and an additional peak is observed at 685 nm, with the 705 nm peak appearing as shoulder. Nevertheless, in dysplastic tissues the 705 nm peak is less prominent and the 685 nm peak appears broadened. Further, the fluorescence intensities at 635, 685 and 705 nm were found to increase with the grade of tissue abnormality. Fig. 6 represents the mean normalized fluorescence spectra for the different grades of DST tissues, viz. healthy, hyperplastic, dysplastic and SCC. We have noticed that for the DST and LST, the peaks at 635, 685 and 705 nm were as intense as that of abnormal sites. Surprisingly, for healthy DST tissues these peaks are more prominent than in SCC. However, as can be seen from figure the emission from abnormal tissues varies according to the grade of tissue abnormality, as observed at buccal and other sites.

Optimum accumulation time for ALA-induced PpIX in abnormal mucosa

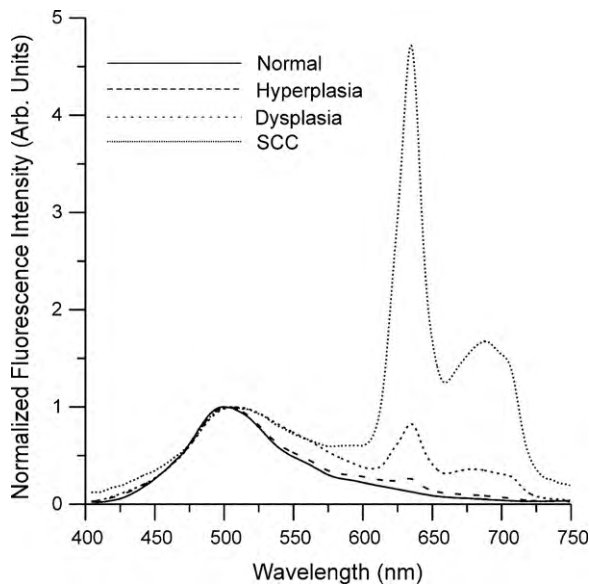Based on the observed optimum accumulation time observed, the anatomical sites can be categorized into two

Figure 5 LIAF emission from different types of oral mucosa from 40 sites in 20 patients and the mean spectra from 13 sites in 36 healthy volunteers, normalized to autofluorescence intensity at 500 nm. Normal spectra represent the average of $36 \times 15 \times 13$ measurements, whereas hyperplasia and dysplasia relate to 9×15 measurements and SCC that of 18×15 measurements.
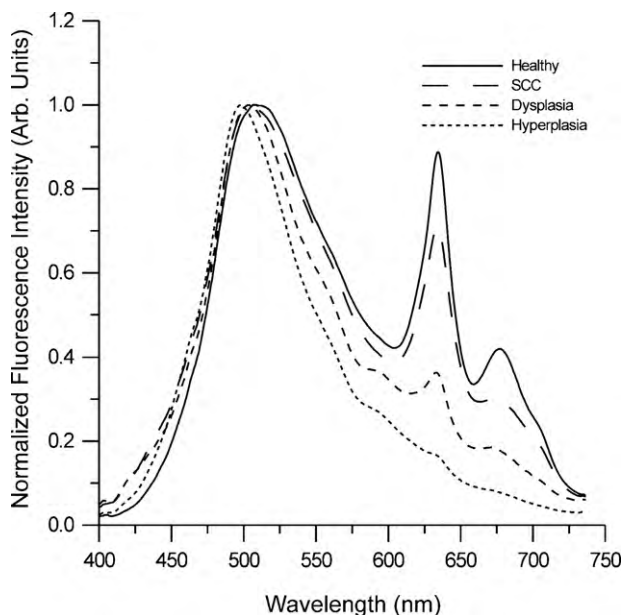

Figure 6 Mean LIAF spectra from different grades of DST tissues normalized to the autofluorescence intensity at 500 nm. Healthy spectra is the average of 36 volunteers, while hyperplastic, dyspalstic and SCC lesions are the average of 4, 7, and 13 patients, respectively. Each spectrum shown is the average of 15 measurements.

groups; one with an accumulation time of 90 min (group I) representing the average of the all sites except DST, LST and VBL and another (group II) with an accumulation time of 150 min representing the average of DST, LST and VBL.

Group I in patient population involves diverse grade lesions of the alveolus, buccal and FM mucosa, whereas, group II consists of LST and DST. As observed in the case of healthy mucosa, in tissues belonging to group I, the maximum accumulation of PpIX occurs at 90 min. Further, after 90 min of ALA application, SCC tissues absorbs PpIX to the maximum, and this accumulation is reflected in the enhanced intensity of 635, 685 and 705 nm peaks, as shown in Fig. 7a—c. Similarly, in the case of group II mucosa, peak accumulation time for different tissue types was observed around 150 min, as shown in Fig. 8a—c.

Figs. 9a—c and 10a—c represent the temporal variation of normalized-fluorescence intensities (NFI) in different abnormal tissue types. As can be seen from these figures both in group I and group II abnormal tissues, these clearing rates are much faster in hyperplastic tissues as compared to dysplastic (pre-malignant) and SCC lesions, which indicates reduced ferrochelatase activity of the heme cycle with increase in tissue abnormality. It could be perceived that in both group I and group II the porphyrin fluorescence intensities show maximum variation from its adjacent tissue grade at the optimum accumulation time and this variation is more prominent at 635 nm. For example, in group I mucosa at the optimal time of 90 min, fluorescence intensity at 635 nm increases by 61% during tissue transformation from dysplasia to SCC and increases by 70% during transformation from hyperplasia to dysplasia. However, corresponding increase for autofluorescence intensity at 635 nm is lower at 50% and 52%, respectively for those tissue transformations. Again, after 120 min of ALA administration the corresponding increase during those transformations are lower than optimum level. A similar trend is observed in group II mucosa.

During the optimal period of 90 min in group I tissues, the enhancement in normalized mean intensity at 635 nm with respect to the autofluorescence intensity was 126.4% in healthy volunteers, whereas in lesions diagnosed as hyperplastic, dysplastic and SCC, the corresponding variations were 223%, 254% and 203%, respectively. Similar trend was observed for the other two peaks at 685 nm and 705 nm. Thus, with ALA application, PpIX emission at 635, 685 and 705 nm gets enhanced both in abnormal and normal mucosa and a higher % variation in intensity indicates higher accumulation of ALA in abnormal tissues.

Conversely, for group II mucosa, the intensity increase with respect to autofluorescence emission at optimal time are 285%, 105%, 367% and 220%, respectively for healthy, hyperplasia, dysplasia and SCC. Contrary to group I, normal mucosa in this case shows higher intensity variations comparable with or even higher than that of benign and abnormal mucosa. This problem arises mainly due to the presence of PpIX-like emission in healthy tissues due to bacterial presence. The intensity enhancements could be much larger if constituents of group II, particularly DST and LST, are considered separately.

Interestingly, the intensity variation of PpIX in group I tissues (Fig. 11a) can be utilized to diagnosis and grade tissues. Although the intensity of the three observed peaks varies with tissue alteration towards malignancy, changes are more prominent in the NFI of the 635 nm red peak (NFI635). Thus, by tracking these NFIs of 635, 685 and 705 nm peaks it is possible to discriminate malignant, pre-malignant, benign tissues from normal. Further, the technique differentiates
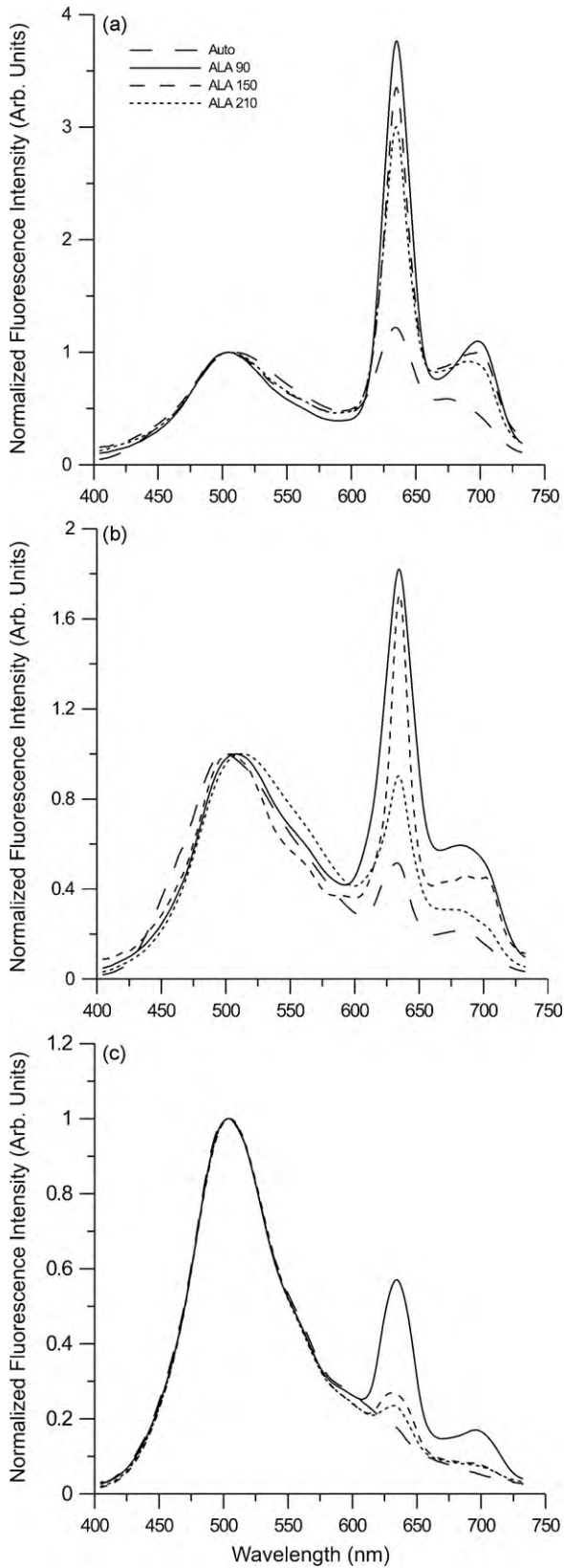
Figure 7 Temporal variation of LIF spectra normalized to the autofluorescence at 500 nm for (a) SCC [*n* = 5], (b) dysplasia [*n* = 5], and (c) hyperplasia [*n* = 5] of group I mucosa for different time periods after the topical administration 5-ALA for 15 min.
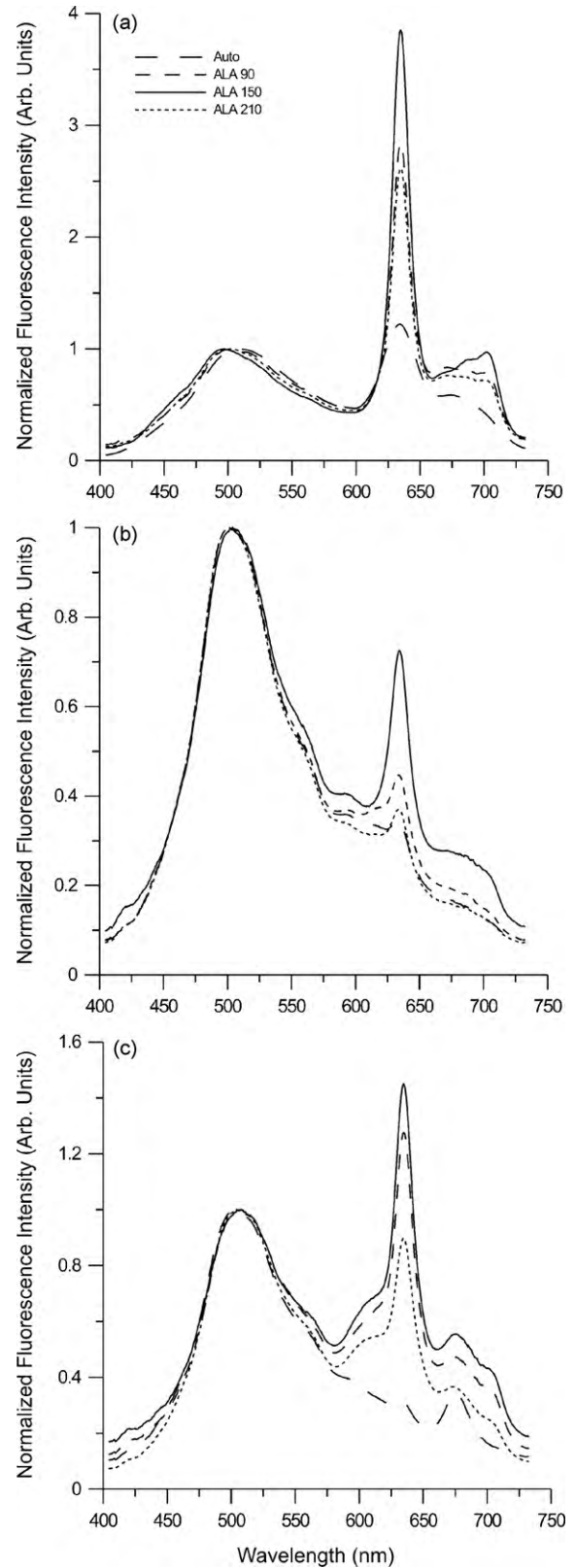
Figure 8 Temporal variation of LIF spectra normalized to the autofluorescence at 500 nm for (a) SCC [*n* = 5], (b) dysplasia [*n* = 5], and (c) hyperplasia [*n* = 5] of group II mucosa for different time periods after the topical administration of 5-ALA for 15 min.

Figure 9 Temporal variation in the mean normalized fluorescence intensities (NFI) at 635, 685 and 705 nm in group I. (a) Hyperplasia, (b) dysplasia and (c) SCC mucosa after the topical administration of 5-ALA for 15 min.
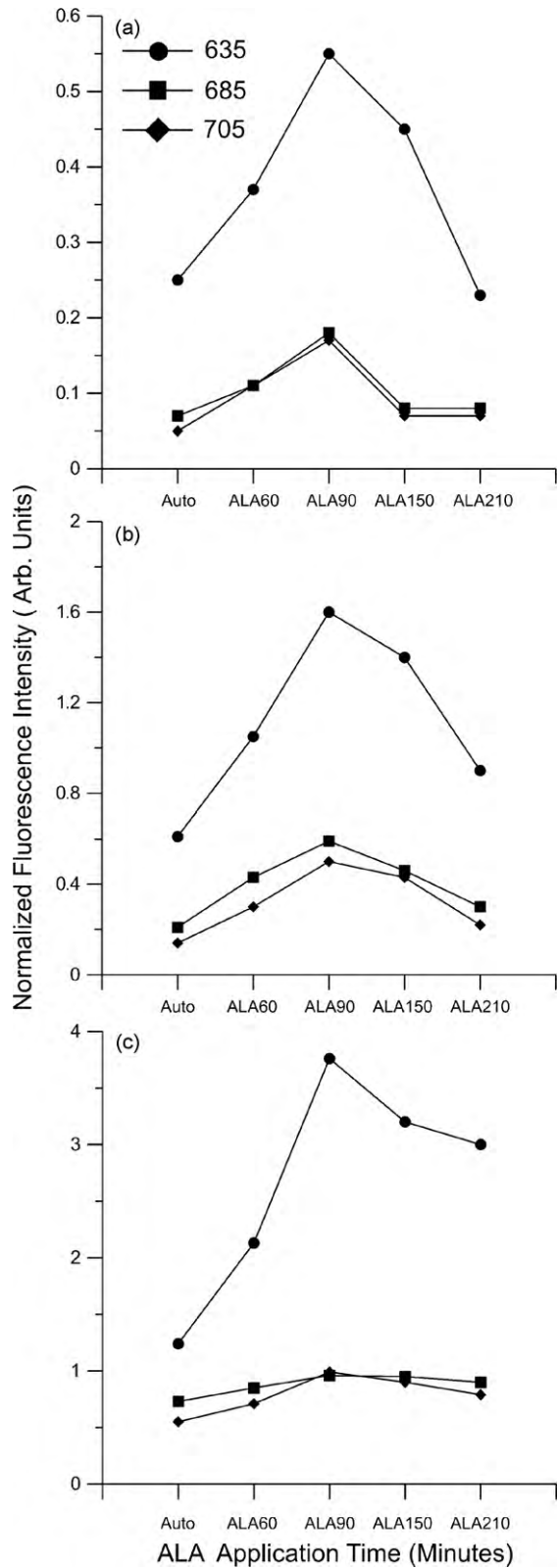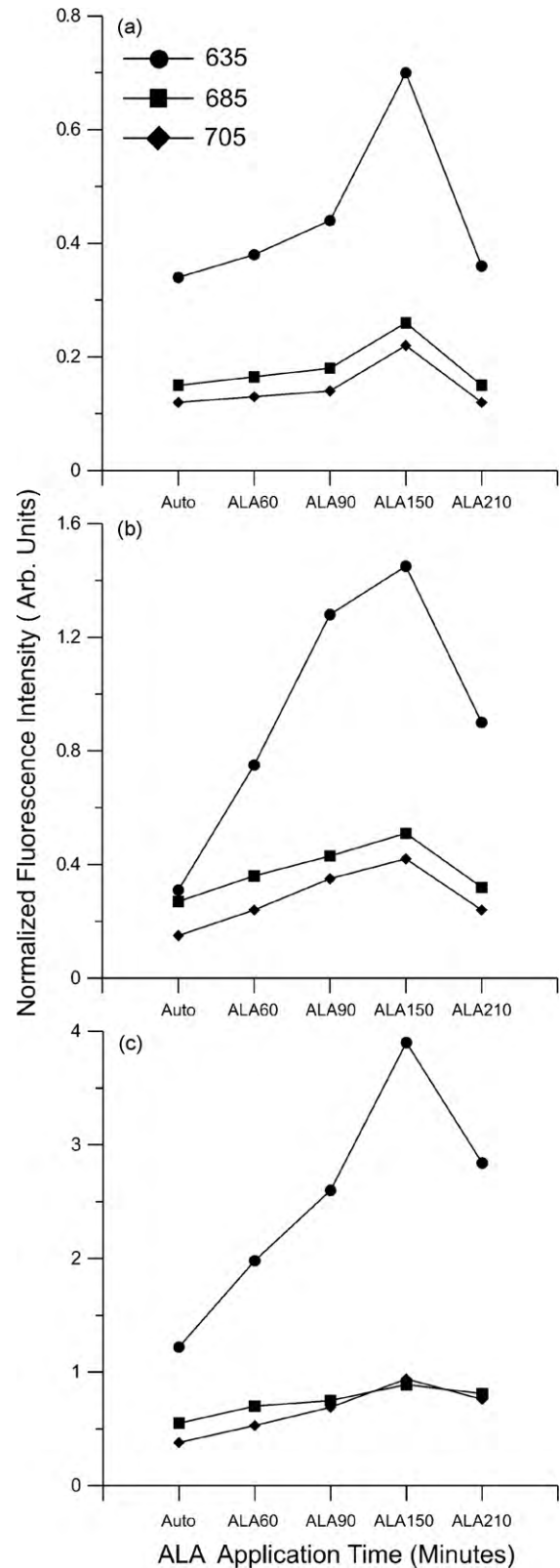
Figure 10 Temporal variation in the mean normalized fluorescence intensities at 635, 685 and 705 nm in group II. (a) Hyperplasia, (b) dysplasia and (c) SCC mucosa after the topical administration of 5-ALA for 15 min.
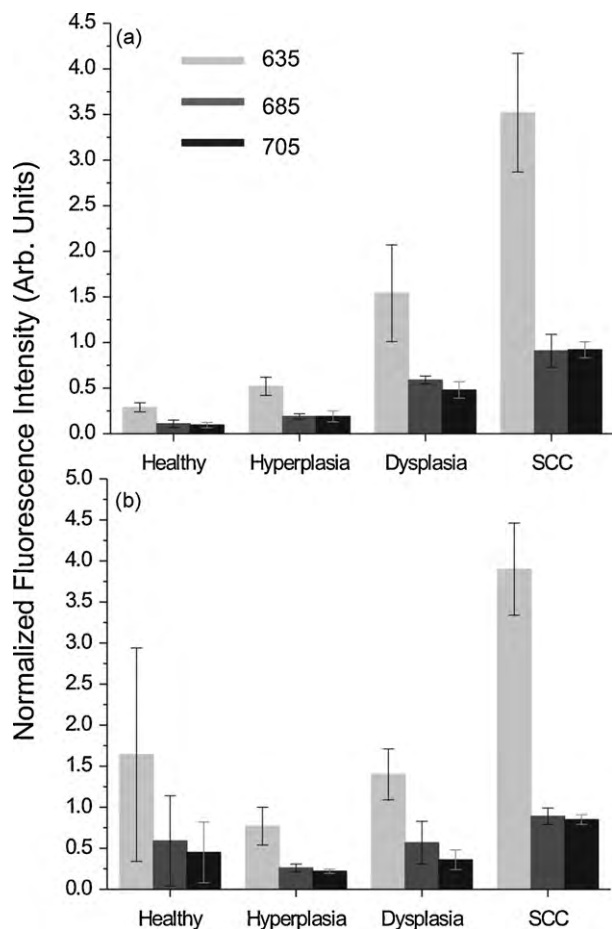
Figure 11 Histogram showing variation in average normalized fluorescence intensities (NFI) at 635, 685 and 705 nm. (a) Group I and (b) group II, at optimal accumulation time after administration of 5-ALA for 15 min.

diverse grades of tissue without any comparison with the normal tissues of the same patient thereby avoiding the possibility of misclassification due to wrong selection of the control site. Table 2 lists the relative NFI (NFI635, NFI685 and NFI705 nm) of the three peaks, with their % variation with respect to control at the optimum accumulation time. However, for group II tissues, it should be noted that the intensities of the major emission bands were found to increase in abnormal tissues (Fig. 11b).

Discussion

LIAF spectral features of healthy and abnormal oral mucosa

The broad autofluorescence emission observed around 500 nm is attributed to endogenous fluorophores, like NADH, FAD, collagen, elastin and amino acids, and the emissions at 635 and 705 nm are from enhanced PpIX presence in the malignant tissues [35,38—45]. The normalized porphyrin emissions in the red region are absent (Fig. 1) in healthy mucosa at sites other than DST, LST and VBL. But as the tissue abnormality increases the emission at 635 and 705 nm starts to dominate the spectra.

By doing such a ''normalization'' of the spectra at 500 nm and by measuring the intensities at 635, 685 and 705 nm, in fact, it is equivalent to measuring the ratios F635/F500, F685/F500 and F705/F500, i.e. red-green fluorescence gating. One of the main advantage of this normalization is that it will help to visualize the variations in the ratios at a peek, as compared raw spectral figures. It has already become known that red to green gating increases the contrast between normal and abnormal. The abovementioned decrease in the green intensity after application of the ALA is dismal as compared to the huge enhancement in the red region. So, we do feel that normalization at the green region is not going to improve the contrast very significantly as dominated by red, but a little bit for sure. However, our actual aim in this study was to track out at what optimal accumulation time this normalization or ratio gives maximum contrast, for the same tissues. Besides, such a normalization (or ratios) provides us a way to reduce the variations associated with spatial non-uniformities in illumination, if any.

In addition to these peaks, we have noticed a prominent peak around 685 nm in SCC tissues that appears between the PpIX emission peaks. In dysplastic tissues, this peak is not very prominent as in SCC, but its presence contributes effectively to broaden of the 705 nm peak. It was noticed that the 685 nm peak is absent in healthy volunteer tissues and in the contra-lateral mucosa of patients and hence cannot be attributed to chlorophyll fluorescence from leafy vegetables or recently consumed food items as proposed earlier [40].

High performance liquid chromatograms of tumor and normal colorectal tissues have shown the presence of a

Table 2 Variation in ALA-induced PpIX intensities at 635, 685 and 705 nm with tissue alterations at optimum accumulation time for group I and group II tissues (%variation from lower grade is shown in parenthesis).

Tissue groups	NFI[a]	Healthy	Hyperplasia	Dysplasia	SCC
Group I	635	0.30	0.50(89.6)	1.60(220)	3.76(135)
	685	0.11	0.18(80)	0.59(227)	0.95(61)
	705	0.09	0.17(89)	0.5(194)	0.99(98)
Group II	635	1.64	0.7(−58)	1.45(107)	3.9(169)
	685	0.60	0.26(−56)	0.51(96)	0.89(75)
	705	0.42	0.22(−51)	0.42(91)	0.94(124)

[a] Normalized fluorescence intensity.

higher concentration of coproporphyrin III in malignant tissues [43,46]. In the same study, peaks at 630 and 685 nm were observed when coproporphyrin III dissolved in methanol was excited with 505 nm light. We therefore propose that the peak observed at 685 nm, especially in SCC and dysplastic tissues, could be due to the accumulation of endogenous fluorophore coproporphyrin III, which is a precursor of PpIX in the heme synthesis.

However, in the healthy tissues of DST, LST and VBL (Fig. 1), the porphyrin-like emission peaks might have originated from bacterial colonization, within the lingual papillary structure of the DST tissues, as described earlier [34]. In such histological structures the chances for deposition and retention of food particles is enormous, making the ground fertile for bacterial colonization [38,40]. Nevertheless, the presence of these peaks leads to erroneous diagnostic results by identifying healthy as abnormal.

Optimum accumulation time for ALA-induced PpIX in healthy and abnormal oral mucosa

It is well known that PpIX selectively accumulates in the abnormal tissues due to the reduced activity of enzymes in the heme biosynthetic pathway [3—5,44,45]. The accumulation and expulsion of PpIX within normal cells can be explained on the basis of heme synthesis as follows.

In every metabolic pathway there is at least one reaction in the cell that is far from equilibrium because of the relatively low activity of the enzyme that catalyzes it. The rate of this reaction is not limited by substrate availability, but only by the activity of this enzyme. The reaction is therefore said to be *enzyme-limited,* and because its rate limits the rate of the whole reaction sequence, this step is known as the *rate-limiting step* in the pathway. In this context, the various biochemical steps in heme cycle are rate limiting, particularly the last three steps. When 5-ALA is given in excess exogenously, the activity of the enzymes gets limited, because of high exogenous input of the substrate and the resulting accumulation of PpIX and its precursors. However in healthy cells, this accumulation is no longer permanent and slowly gets washed out by conversion to PpIX and then to heme with time.

Even though the epithelium is stratified throughout the oral cavity, the mucous membrane differs in morphology at different sites. This definitely affects the diffusion of ALA into the cells during topical application. Particularly, in the case of DST and LST, the papillary structure of mucosa facilitates longer retention of ALA solution and increases the accumulation time leading to larger PpIX intensities. Similar results were observed in a model study on nude mouse skin using 10% (w/w) ALA and hexyl esters of ALA wherein the 635 nm intensity increased to its maximum with increasing administration time [47]. Further, it was reported that with increase in administration time the optimum accumulation time also increased. However, in flat non-papillary structures associated with other types of lining mucosa the possibility for deposition is low.

Superficial layer of epidermis reduces the diffusion rate of ALA across the stratum corneum [48]. Therefore, the thicker lingual structure and superficial keratin layer of DST and LST sites results in slower uptake. On the other hand, VBL, which is the transitional zone between the lip skin and mucous membrane of the lips, is covered by a moderately thick keratinized epithelium with a rather thick stratum corneum. The presence of these two layers together slows down the uptake of the 5-ALA as compared to inner lip or other lining mucosa. For all healthy anatomical sites, the intensity of PpIX emission decreases with time showing the temporal elimination of ALA from body (Fig. 4a—d).

Diagnosis based on optimum accumulation time of normalized fluorescence

In normal epithelial tissues, the superficial stratum corneum layer is the main barrier against the diffusion of ALA [47]. The stratum corneum consists of keratin layers (corneocytes) embedded in a lipid matrix. There are two ways for diffusion through the stratum corneum; across the corneocytes (trancellular) or via lipid matrix (intercellular) [47—49]. The latter route is believed to be the principal pathway and thus, the major barrier for permeation [50,51]. Since pre-malignant and malignant lesions usually associate with hyperkeratosis, higher optimum time periods could be expected in these lesions. However, similar optimal times observed in the pre-malignant and malignant lesions could be explained as due to the cutaneous stratum corneum. Eventhough thicker hyperkeratic layer limits the diffusion, at the same time, the disorder produced in the lipids within the intercellular space permits the diffusion through stratum corneum. After reaching the optimal accumulation period in both groups I and II, the PpIX intensity shows a decreasing or constant trend indicating the clearance of ALA-induced PpIX from the system.

The variation of NFI in group I tissues (Fig. 11a) can be utilized to diagnosis and grade tissues. Although the intensity of the three observed peaks varies with tissue alteration towards malignancy, changes are more prominent in the red NFI 635 nm peak. Zeng et al. has used the red-green intensity ratio to differentiate different grades oral tissues using an endoscopic imaging system after topical application of 0.4% solution of 5-ALA [24]. The malignant lesions (including CIS and SCC) showed a maximum increase of 294%, while pre-malignant dysplasia and benign hyperplasia/inflammatory mucosa showed variations of 200% and 100%, respectively from normal values in 240 min of ALA application. In contrast, the corresponding increases reported in this study are very much higher at 1196%, 537% and 90%, respectively. The lower variations reported earlier might be due to the inclusion of tongue tissues in their algorithms, where the possibility of false diagnosis is too high to affect the overall diagnostic accuracy.

For group II, in abnormal tissues (Fig. 11b) the intensity variation is prominent at NFI635, with SCC and dysplasia showing variations of 413% and 91%, respectively. As against the increasing trend seen in group I mucosa, there is a decreasing trend during transition from normal to hyperplasia in group II (Table 2). In other words, in group II, tissues that were pathologically identified as hyperplasia were indistinguishable from normal from fluorescence intensity variations.

Table 3 Comparison of diagnostic accuracies in terms of ROC-AUCs of three fluorescence intensities for group I and group II in discerning different tissues types.

Tissue groups	Spectral intensities	ROC-AUC			
		Healthy vs. hyperplasia	Hyperplasia vs. dysplasia	Dysplasia vs. SCC	Overall accuracy
Group I	F635	0.96	0.96	1.00	0.97
	F685	0.92	1.00	0.84	0.92
	F705	0.97	0.98	0.94	0.96
	Mean	0.95	0.98	0.93	0.95
Group II	F635	—	0.98	1.00	0.99
	F685	—	0.96	0.82	0.89
	F705	—	0.84	0.90	0.87
	Mean	—	0.93	0.91	0.92

Evaluation of diagnostic accuracy using ROC-curve analysis

SPSS (Version 10) software was used to compare the area under different curves (AUC) and to check the efficacy of different methodologies without being constricted to single values of sensitivity and specificity. It calculates the sensitivity and specificity of given input values and plots the ROC curves, with sensitivity values against the values of (1-specificity). For both tissue groups I and II, the classification of different grades oral mucosa was successful with very good values of ROC-AUC. Table 3 shows ROC-curve plotted using sensitivity and specificity values attained for optimal ALA-induced fluorescence intensities (F635, F685, and F705). For group I mucosa, the discrimination of different tissue types was possible, with ROC-AUCs in the range 0.84—1. However, for the relevant clinical challenge of discriminating hyperplasia from dysplasia using F635 and F705 intensities the ROC-AUCs were 0.96 and 0.98, respectively, while for the F685 a perfect discrimination was possible with ROC-AUC of 1. In comparison de Veld et al. had obtained a ROC-AUC < 0.65 to differentiate hyperplasia tissues from dysplasia using a different combination of normalization methods and classifiers [30]. In the same study, an improved ROC-AUC of 0.70—0.77 was reported to discriminate these tissues using diffuse reflectance spectral features.

The overall mean ROC-AUC for the 635, 685 and 705 nm peak NFIs at the optimal accumulation time to differentiate the three tissue types in group I mucosa was 0.95, while for group II mucosa it was 0.92. These results show the advantage of ROC-curve analysis in determining diagnostic accuracies during cancer diagnosis. The basic motivation of this statistical study is to show statistical significance of the results. It should be noted that this is only was preliminary phase of study and the number of available sites in each tissue categories are low, particularly, as we are dividing them in four tissue categories, i.e. normal, hyperplastic, dysplastic and SCC (Instead of simply dividing these categories to normal and abnormal). This particular constraint not allowed us to attempt the training and evaluation statistical approach.

Conclusions

Maximum accumulation of ALA-induced PpIX fluorescence at different anatomical sites of the oral cavity in healthy population and in different grades of abnormal oral tissues was determined *in vivo* by tracking the emission peak intensities 635, 685 and 705 in the normalized LIAF spectra. The normalized fluorescence intensities were found to peak within 90—150 min of administration depending on the anatomical location, both in healthy and abnormal tissues. In group I oral mucosa that involves all anatomical sites excepting the DST, LST and VBL, the intensities at 635, 685 and 705 show an increasing trend during tissue transformation from healthy to SCC. Among the three peak optimal intensities studied, the F635 was found to be more sensitive to tissue characteristics. In the group II mucosa consisting of DST, LST and VBL, the normalized intensities of the three peaks increased according to the grade of abnormal tissue. However, a decreasing trend was noticed in the normalized intensities during transformation to hyperplasia. This trend reversal in healthy tissues could possibly lead to misclassification of normal tissues as benign (hyperplasia), dysplasia or SCC, particularly in the case of DST and LST where these emissions are more intense than in VBL. This would also increase the number of false positives thereby decreasing the specificity of the diagnostic technique. Nonetheless, in both group I and group II abnormal tissues, the porphyrin NFIs show maximum variation with respect to the adjacent grade, at the optimum accumulation time. Though the patient population is limited, the study confirms the significance of carrying out *in vivo* ALA-induced PpIX fluorescence measurements at the optimum accumulation time to improve the capability for early detection and grading of oral cancer. The major clinical challenge of discriminating oral dysplasia from hyperplasia was achieved with an ROC-AUC of 1. The observed overall ROC-AUCs of 0.95 and 0.92 in discriminating different types of group I and group II oral mucosa show the advantages of recording ALA-induced porphyrins intensities at the optimal time and calls for a prospective study in a larger patient population through community centers. In short, it could be concluded that by optimizing the accumulation time after application of ALA the contrast and accuracy of the ALA-PD in oral cancer detection can be

improved. Further, the knowledge of the this optimum accumulation time and high tissue selectivity of PpIX in abnormal tissues offers opportunities for therapeutic approach using PDT in future and towards this, the knowledge of optimal ALA concentration is at different anatomical sites becomes vital.

Point spectroscopy is an adequate technique for quantifying PpIX fluorescence. However, point monitoring spectroscopy has the disadvantage that it gives no information on the spatial distribution of PpIX fluorescence within a lesion. We have surmounted this concern by restricting our measurements within small margined lesion areas. Again, another limitation associated with point monitoring is that it takes a lot of time to scan of an entire lesion point by point, which could be overcome with the use of multispectral imaging systems based on expensive intensified CCD (ICCD) or EMCCD cameras that can gather fluorescence images of the entire lesion in a diminutive time frame, which could helps to distinguish the spatial distribution of PpIX fluorescence in real time.

Acknowledgements

References

[1] Forlay J, Parking DM, Pissani P. Globscan 2002: cancer incidence mortality and prevalence worldwide. Lyon IARC Publication/France; 2007.

[2] Date M, Sakata I, Fukuchi K, et al. Photodynamic therapy for human oral squamous cell carcinoma and xenografts using a new photosensitizer. Lasers Surg Med 2003;33:57—63.

[3] Peng Q, Warloe T, Berg K, et al. 5-Aminolevulinic acid-based photodynamic therapy-clinical research and future challenges. Cancer 1997;79(12):2282—308.

[4] Rubino GF, Rasetti L. Porphyrin metabolism in human neoplastic tissues. Panminerva Med 1996;8:290—2.

[5] Kondo M, Hirota N, Takaoka T, Kajiwara M. Heme-biosynthesis enzyme activities and porphyrin accumulation in normal liver and hepatoma cell line of rats. Cell Biol Toxicol 1993;9:95—105.

[6] Webber J, Kessel D, Fromm D. Side effects and photosensitization of human tissue after aminolevulinic acid. J Surg Res 1997;68:31—7.

[7] Vogl TJ, Eichler K, Mack MG, et al. Interstitial photodynamic laser therapy in interventional oncology. Eur Radiol 2004;14:1063—73.

[8] Sorenson R, Juzenas P, Iani V, Moan J. Formation of protoporphyrin IX in mouse skin after topical application of 5-ALA and its methyl ester. Proc SPIE 1999;3563:77—81.

[9] Van der Veen N, de Bruijn HS, Berg JW, Star WM. Kinetics and localization of PpIX fluorescence after topical and systemic ALA application, observed in skin and skin tumors of UVB-treated mice. Br J Cancer 1996;73:925—30.

[10] Peng Q, Warloe T, Moan J, et al. Distribution of 5-ALA-induced porphyrins in nodulo-ulcerative BCC. Photochem Photobiol 1995;62:906—13.

[11] Messmann H. 5-ALA induced PpIX for the detection of gastrointestinal dysplasia. Gastrointest Endosc Clin N Am 2000;10:497—512.

[12] Messmann H, Endlicher E, Freunek G, Rummele P, Scholmerich J, Kruchel R. Fluorescence endoscopy for the detection of low and high grade dysplasia in ulcerative colitis using systemic or local 5-ALA sensitization. Gut 2003;52:1003—7.

[13] Af Klitenberg C, Enejeder AMK, Wang I, Andersons-Engels S, Svanberg S, Svanberg K. Kinetic fluorescence studies of 5-aminolevulinic acid-induced PpIX accumulation in BCC. J Photochem Photobiol B 1999;49:120—8.

[14] Ogasawara T, Miyoshi N, Sano K, et al. Influence of administration methods on the accumulation of ALA-induced PpIX in mouse tongue tumors. Oral Dis 2006;12:415—9.

[15] Vaidyanathan V, Rastegar S, Fossum TW, et al. In vitro kinetics of ALA-induced fluorescence in the canine oral cavity: influence of drug dose and tissue type. Proc SPIE 1997;2975: 222—6.

[16] Grant WE, Hopper C, MacRobert AJ, Speight PM, Bown SG. Photodynamic therapy of oral cancer: photosensitization with systemic ALA. Lancet 1993;342:147—8.

[17] Fan k, Hopper C, Speight P, Bown S. Aminolevulinic acid as a photosensitizer for PDT of oral dysplasia. In: Proceedings of British society for dental research the British division of the IADR 44th annual meeting. 1996.

[18] De Rosa FS, Maechetti JM, Thomazini JA, Tedesco AC, Bentley MVLB. A vehicle for photodynamic therapy of skin cancer: influence of dimethylsulphoxide on 5-ALA in vitro cutaneous permeation and invivo PpIX accumulation determined by confocal microscopy. J Control Release 2000;65:359—66.

[19] van der Akker JTHM, Lani V, Star WM, et al. Topical application of 5-aminolevulinic acid hexyl ester and 5-aminolelulinic acid to normal nude mouse skin: differences in PpIX fluorescence kinetics and role the stratum corneum. Photochem Photobiol 2003;72:681—9.

[20] Betz CS, Stepp H, Janda P, et al. A comparative study of normal inspection, autofluorescence and 5-ALA-induced PpIX fluorescence for oral cancer diagnosis. Int J Cancer 2002;97(2):245—52.

[21] Leunig A, Rick K, Stepp H, et al. Fluorescence imaging and spectroscopy of 5-aminolevulinic acid induced PpIX for the detection of neoplastic lesions in the oral cavity. Am J Surg 1996;172(6):674—7.

[22] Leunig A, Betz CS, Mehlmann M, et al. Detection of squamous cell carcinoma of the oral cavity by imaging 5-amino levulinic acid-induced protoporphyrin IX fluorescence. Laryngoscope 2000;110:78—83.

[23] Stolic S, Tomas SA, Roman-Gallegos E, et al. Kinetic study of 5-ALA induced porphyrins in mice using photoacoustic and fluorescence spectroscopies. J Photchem Photobiol B 2002;68:122—7.

[24] Zheng W, Khee CS, Ranjiv S, Malini O. Detection of neoplasms in the oral cavity by digitized endoscopic imaging of 5-aminolevulinic acid-induced protoporphyrin IX fluorescence. Int J Oral Onc 2002;21:763—8.

[25] Zheng W, Khee CS, Ranjiv S, Malini O. Detection of squamous cell carcinoma and pre-cancerous lesions of the oral cavity by quantification of 5-aminolevulinic acid induced fluorescence endoscopic images. Lasers Surg Med 2006;31(3):151—7.

[26] Rupananda JM, Subhash N, Anitha M, et al. Laser induced autofluorescence spectral ratio standard for early detection of oral cancer. Head Neck 2010;32(6):763—79.

[27] Rupananda JM, Shiny ST, Rejnish Kumar R, et al. Laser induced autofluorescence spectral ratio standard for early detection of oral cancer. Cancer 2008;112(7):1503—12.

[28] Diamond KR, Farrell TJ, Patterson MS. Measurement of flurophores concentrations and fluorescence quantum yield in tissue-simulating phantoms using three diffusion models of steady state spatially resolved fluorescence. Phys Med Biol 2003;48(24):4135—49.

[29] Muller MG, Georgakoudi I, Zhang Q, Feld MS. Intrinsic fluorescence spectroscopy in turbid media: disentangling effects of scattering and absorption. Appl Opt-OT 2001;40(25):4633—46.

[30] De Veld CDCG, Skurichina M, Witjes MJH, Duin RPW, Sterenborg HJCM, Roodenburg JLN. Autofluorescence and diffuse reflectance spectroscopy for oral oncology. Lasers Surg Med 2005;36(5):356—64.

[31] Zweig MH, Campbell G. Receiver-operating characteristic (ROC) plots; a fundamental evaluation tool in clinical medicine. Clin Chem 1993;39:561—77.

[32] Griner PF, Mayewski RJ, Mushlin AI, Greenland P. Selection and interpretation of diagnostic tests and procedures. Ann Intern Med 1981;94:555—600.

[33] Metz CE. Basic principles of ROC curve analysis. Semin Nucl Med 1978;8(4):283—98.

[34] Leunig A, Rick K, Stepp H, Goetz A, Baumgartner R, Fey J. Photodynamic diagnosis of neoplasms of the mouth cavity after local administration of 5-aminolevulinic acid. Laryngorhinootologie 1996;75(8):459—64.

[35] Sharwani A, Jerjes W, Salih V, et al. Fluorescence spectroscopy combined with 5-aminolevulinicacid-induced protoporphyrin IX fluorescence in detecting oral premalignancy. J Photochem Photobiol B 1996;83:27—33.

[36] Suhr MAA, Hopper C, Jones L, George JGD, Bown SD, MacRobert. Optical biopsy system for the diagnosis and monitoring of superficial cancer and precancer. Int J Oral Maxillofac Surg 2000;29:453—7.

[37] Riedl CR, Daniltchenko D, Koenig F, Simak R, Koening SA, Pflueger H. Flurescence endoscopy with 5-ALA reduced early recurrence rate in superficial bladder cancer. J Urol 2001;165:1121—3.

[38] Da Costa RS, Anderson H, Wilson B. Molecular fluorescence excitation-emission matrices relevant to tissue spectroscopy. Photochem Photobiol 2003;78:384—92.

[39] Drezek R, Sokolov K, Utzinger U, et al. Understanding the contributions of NADH and Collagen to cervical tissue fluorescence spectra: modeling, measurements, and implications. J Biomed Opt 2001;6:385—96.

[40] Ingrams DR, Dingra JK, Roy K, et al. Autofluorescence characteristics of oral mucosa. Head Neck 1997;19:27—32.

[41] Richards-Kortum R, Sevick-Muraca E. Quantitative optical spectroscopy for tissue diagnosis. Ann Rev Phys Chem 1996;7:555—606.

[42] De Veld DCG, Marina S, Witijes MJH, et al. Autofluorescence characteristics of healthy oral mucosa at different anatomical sites. Lasers Surg Med 2003;23:367—76.

[43] Moesta KT, Bernd E, Tim H, et al. Protoporphyrin IX occurs naturally in colorectal cancers and their metastases. Cancer Res 2001;61:991—9.

[44] Leibovici L, Schoenfeld NILI, Yehoshua HA, et al. Activity of porphobilinogen deaminase in peripheral blood mononuclear cells of patients with metastatic cancer. Cancer 1988;62:2297—300.

[45] Peng Q, Warloe T, Berg K, et al. 5-Aminolevulinic acid based photodynamic therapy: principles and experimental research. Photochem Photobiol 1997;65:235—51.

[46] Dietel W, Bolsen K, Dickson E, Fritsch C, Pottier R, Wendenburg R. The formation of water-soluble porphyrins and protoporphyrinIX in 5-aminolevulinic acid incubated carcinoma cells. J Photochem Photobiol B 1996;33:225—31.

[47] Van den Akker JTHM, Iani V, Star WM, Sterenborg HJCM, Moan J. Topical application of 5-aminolevulinic acid hexyl ester and 5-aminolevulinic acid to normal nude mouse skin: differences in PpIX fluorescence kinetics and the role of the stratum corneum. Photochem Photobiol 2000;72:681—9.

[48] Landmann L. The epidermal permeability barrier. Anat Embryol 1988;178:1—13.

[49] Menton DN, Eisen AZ. Structure and organization of mammalian stratum corneum. J Ultrastruct Res 1971;35:247—64.

[50] William AC, Barry BW. Skin absorption enhancer. Crit Rev Ther Drug Carrier Syst 1992;9:305—53.

[51] Suhonen ATM, Bouwstra JA, Urtti A. Chemical enhancement of precutaneous absorption in reaction to stratum corneum structural alterations. J Control Release 1999;59:149—61.